Two-neutron correlations in ^{6}He in a Coulomb breakup reaction

Yuma Kikuchi* and Kiyoshi Katō†
Division of Physics, Graduate School of Science, Hokkaido University, Sapporo 060-0810, Japan

Takayuki Myo‡
General Education, Faculty of Engineering, Osaka Institute of Technology, Osaka 535-8585, Japan and
Research Center for Nuclear Physics (RCNP), Osaka University, Ibaraki 567-0047, Japan

Masaaki Takashina§
Department of Medical Physics and Engineering, Graduate School of Medicine, Osaka University, Suita 565-0871, Japan and
Research Center for Nuclear Physics (RCNP), Osaka University, Ibaraki 567-0047, Japan

Kiyomi Ikeda‖
The Institute of Physics and Chemical Research (RIKEN), Wako 351-0198, Japan
(Received 14 December 2009; revised manuscript received 23 February 2010; published 16 April 2010)

We investigate the three-body Coulomb breakup of a two-neutron halo nucleus, ^{6}He. Based on the $\alpha + n + n$ model, the three-body scattering states of ^{6}He are described by using the combined methods of the complex scaling and the Lippmann-Schwinger equation. We calculate the breakup cross section, the two-dimensional energy distributions, and the invariant mass spectra for the $E1$ transition of ^{6}He. We discuss the relations between the structures in these strengths and the n-n and α-n correlations of ^{6}He. It is found that the ^{5}He resonance in the final states contributes to make a low-energy enhancement of the strength. The n-n final-state interaction also contributes to enhance the strength globally. However, the ground-state correlations of ^{6}He, such as a dineutron, are difficult to recognize in the strength because of the dominant effect of the final-state interaction.

DOI: 10.1103/PhysRevC.81.044308 PACS number(s): 21.60.Gx, 21.10.Pc, 25.60.Gc, 27.20.+n

I. INTRODUCTION

Since the discovery of neutron halo nuclei such as ^{6}He, ^{11}Li, and ^{11}Be, extensive studies have been performed to understand their exotic structures caused by the enormously weak binding of the valence neutrons.

Theoretically, using the models based on the core + valence neutrons picture, the halo structure of the ground states and their excitations have been investigated [1–7]. In two-neutron halo nuclei it has been pointed out that the correlation between two neutrons causing the halo structure is important in reproducing the observed small two-neutron separation energies and large matter radii [3–5]. This n-n correlation has been also shown to be well described by the mixing of many $J^\pi = 0^+$ pairing configurations with large orbital angular momenta. The core $+ n + n$ three-body model calculations indicate that the n-n correlation is characterized as the spatial localization in the density distribution, the so-called "dineutron" [1,4,6,8].

Many experiments have been also performed to expose the role of the n-n correlation in the two-neutron halo nuclei [9–14]. The Coulomb breakup reactions using a high-Z target such as Pb provided us with interesting information on the weakly binding properties and the excitations of halo nuclei. For example, the characteristics of the dipole ($E1$) excitation have attracted much attention, because the $E1$ response is considered to be dominant in the Coulomb breakup reaction. It is also expected to gain a deeper understanding of the n-n correlation in the two-neutron halo nuclei through the Coulomb breakup reactions [15–18]. However, the nature of the Coulomb breakup of the two-neutron halo nuclei is still unclear because the two-neutron halo nuclei are broken up to the three-body scattering states and the binary subsystems can form the resonances and virtual states in the final states. To understand the n-n correlation in the two-neutron halo nuclei, there are at least three problems to be solved: (i) clarifying the dominant breakup process such as the direct breakup to a non-interacting three-body continuum or sequential decay via the resonance of the binary subsystem, (ii) evaluating the influence of the final-state interactions (FSI) on the cross section, and (iii) specifying the kinematical conditions of the three-body breakup.

In our previous works [7,19], we have described the two-neutron halo nuclei with the core $+ n + n$ three-body model, where the core nucleus is expressed by the multiconfigurations taking into account not only the pairing correlation but also the tensor correlation for ^{6}He and ^{11}Li. Combining this three-body model with the complex scaling method (CSM), we have succeeded in explaining the observed Coulomb breakup cross sections of halo nuclei [8,20,21]. Based on those results, in this article we perform an extensive analysis to investigate the structure of the $E1$ strengths of the halo nucleus ^{6}He. In particular, we investigate the effects of the n-n and α-n correlations of ^{6}He on the strength distributions.

Recently, we have developed a method to describe the three-body scattering of nuclei, in which the complex scaling

*yuma@nucl.sci.hokudai.ac.jp
†kato@nucl.sci.hokudai.ac.jp
‡myo@ge.oit.ac.jp
§takasina@rcnp.osaka-u.ac.jp
‖k-ikeda@apricot.ocn.ne.jp

and the Lippmann-Schwinger equation are combined. We refer to this new approach as the complex-scaled solutions of the Lippmann-Schwinger equation (CSLS) [22]. In CSLS, every correlation in the three-body scattering states is taken into account explicitly in the Green's function of the core $+ n + n$ system. The advantages of CSLS are follows: First, CSLS provides us with the accurate three-body scattering solutions, which satisfy the outgoing boundary conditions of three-body decay. Second, the eigenstates of every binary subsystem, such as the core-n and n-n for the core $+ n + n$ system, are expressed as functions of the energies of the subsystem in the asymptotic region. Hence, we can describe the Dalitz plot of the breakup strength as functions of the observed subsystem energies and can discuss the existence of the subsystem correlations from the strength. Finally, the influence of FSI can be discussed using the obtained breakup strength. We have applied this CSLS method to the three-body Coulomb breakup reaction of ^{6}He [22] and successfully reproduced the observed breakup cross section. This result showed the reliability of CSLS to describe the three-body breakup reaction of halo nuclei.

In this study, we perform the detailed analysis of the $E1$ excitation of ^{6}He using the three-body CSLS method. We aim to clarify the relation between the subsystem correlations of α-n and n-n and the structure appearing in the $E1$ strengths. For this purpose, we evaluate the two-dimensional energy distributions of the $E1$ strength of ^{6}He and also the corresponding invariant mass spectra. These distributions are the functions of the relative energies of the n-n and α-n subsystems and give us the physical information to examine the subsystem correlations of ^{6}He. The invariant mass spectra are compared with the experimental data. We examine whether the signatures of the ground-state correlations of ^{6}He, such as di-neutrons, can be observed in the strengths. We further discuss the effects of FSI on the strengths.

This article is organized as follows. In Sec. II, we explain our theoretical framework: the core $+ n + n$ three-body model, CSM, and the CSLS method for three-body breakup. In Sec. III, we show the results of the Coulomb breakup strength of ^{6}He and discuss the structure appearing in the various strength distributions. All results and discussions are summarized in Sec. IV.

II. METHOD

A. $\alpha + n + n$ three-body model of ^{6}He

We give a brief explanation of the $\alpha + n + n$ three-body model of ^{6}He. The detailed explanation of this model is given in Refs. [5,20]. In this model, an α core is described as the $(0s)^4$ configuration, whose oscillator length b_c, is taken as 1.4 fm to reproduce the charge radius. The effect of the antisymmetrization between the α core and a valence neutron is treated in the orthogonality condition model [23], in which the Pauli forbidden states are excluded in the relative motions of the $\alpha + n + n$ system. The total wave function of ^{6}He with the state J^π is expressed as

$$\Phi^{J^\pi}(^6\mathrm{He}) = \Phi(\alpha)\chi^{J^\pi}(nn), \tag{1}$$

where the wave function of the α core is expressed as $\Phi(\alpha)$. The relative wave function of valence neutrons is $\chi^{J^\pi} = \chi^{J^\pi}(nn)$. To obtain χ^{J^π}, we solve the following Schrödinger equation:

$$\hat{H}\chi^{J^\pi} = E\chi^{J^\pi}, \tag{2}$$

where E is the energy eigenvalue measured from the $\alpha + n + n$ threshold. The Hamiltonian for the relative motion is expressed as

$$\hat{H} = \sum_{i=1}^{3} t_i - T_{\mathrm{c.m.}} + \sum_{i=1}^{2} V_{\alpha n}(\mathbf{r}_i) + V_{nn} + V_{\alpha nn} + V_{\mathrm{PF}}. \tag{3}$$

The operators t_i and $T_{\mathrm{c.m.}}$ are kinetic energies of each particle and a center-of-mass motion of the three-body system, respectively. For interactions, the microscopic KKNN potential [24] and the effective Minnesota potential [25] are used as $V_{\alpha n}$ and V_{nn}, respectively. The coordinate $\mathbf{r}_i$ ($i = 1$ or 2) represents a relative coordinate between the α core and each valence neutron. In this model, to reproduce the threshold energy of the $\alpha + n + n$ breakup from the ground state of ^{6}He, we introduce the effective αnn three-body interaction $V_{\alpha nn}$ [19,20], which is given as

$$V_{\alpha nn} = V_3 e^{-\nu(\mathbf{r}_1^2 + \mathbf{r}_2^2)}, \tag{4}$$

where $V_3 = -1.503$ MeV and $\nu = 0.07/b_c^2$ fm^{-2}.

For the valence neutrons of ^{6}He, the Pauli forbidden state ϕ_{PF} is the $0s$ orbits occupied by the α core. This $0s$ component is excluded from the relative motion of the $\alpha + n + n$ system by using the so-called pseudopotential V_{PF} defined as

$$V_{\mathrm{PF}} = \lambda|\phi_{\mathrm{PF}}\rangle\langle\phi_{\mathrm{PF}}|, \tag{5}$$

where λ is taken as 10^6 MeV in the numerical calculation.

The relative motion in the $\alpha + n + n$ system is obtained by solving Eq. (2) accurately with a few-body technique. Here we employ the variational approach called the hybrid-VT model [5]. In this model, a relative wave function χ^{J^π} of the $\alpha + n + n$ three-body system is expanded with two types of basis function: One is the cluster orbital shell model (COSM; V-type) and the other is the extended cluster model (ECM; T-type). Combining these basis functions, the relative wave function is described as

$$\chi^{J^\pi} = \chi_{\mathrm{V}}^{J^\pi}(\boldsymbol{\xi}_{\mathrm{V}}) + \chi_{\mathrm{T}}^{J^\pi}(\boldsymbol{\xi}_{\mathrm{T}}), \tag{6}$$

where $\chi_{\mathrm{V}}^{J^\pi}$ ($\chi_{\mathrm{T}}^{J^\pi}$) expresses the relative wave function of V-type (T-type) and $\boldsymbol{\xi}_{\mathrm{V}}$ ($\boldsymbol{\xi}_{\mathrm{T}}$) is a V-type (T-type) relative coordinate set. These two kinds of basis states are important for expressing the α-n and n-n correlations simultaneously. Radial components of each relative wave function are expanded using Gaussian basis functions [26]. The number of basis functions is determined to reach the convergence of the obtained results.

B. Complex scaling method

We explain the CSM to describe the three-body scattering states. In CSM [27,28], the relative coordinates are transformed as follows:

$$U(\theta)\boldsymbol{\xi}U^{-1}(\theta) = \boldsymbol{\xi}e^{i\theta}, \tag{7}$$

where $U(\theta)$ is a complex scaling operator with a scaling angle θ being a real number. Applying this transformation to the Hamiltonian $\hat{H}$, we obtain the complex-scaled Hamiltonian $\hat{H}^\theta = U(\theta)\hat{H}U^{-1}(\theta)$. The transformed Schrödinger equation for $\hat{H}^\theta$ corresponding to Eq. (2) is expressed by

$$\hat{H}^\theta \chi^\theta = E^\theta \chi^\theta, \tag{8}$$

where χ^θ is a complex-scaled wave function given as

$$\chi^\theta = U(\theta)\chi(\boldsymbol{\xi}) = e^{(\frac{3}{2}i\theta)f}\chi(\boldsymbol{\xi}e^{i\theta}). \tag{9}$$

The factor $e^{(\frac{3}{2}i\theta)f}$ in Eq. (9) comes from a Jacobian for a volume integral with f degrees of freedom ($f = 2$ for a three-body system). By solving the complex-scaled Schrödinger equation of Eq. (8) with a finite number of L^2 basis functions, we obtain the eigenstates and energy eigenvalues of $\hat{H}^\theta$ as $\{\chi_n^\theta\}$ and $\{E_n^\theta\}$ with a state index n, respectively.

All the energy eigenvalues $\{E_n^\theta\}$ are obtained on a complex energy plane, governed by the ABC theorem [28]. In the ABC theorem, it is proved that the energies of bound states are given by real numbers and are invariant by complex scaling. However, those of resonances and continuum states are complex values. Energies of resonances are given by $E_n^\theta = E_n^r - i\Gamma_n/2$, which are independent of θ. The resonance energies E_n^r are measured from the threshold and Γ_n are decay widths. Energies of continuum states are obtained on branch cuts of the Riemann sheet, which are rotated down by 2θ from the real axis. Because the behavior of the resonances and continuum energies are different, by adopting a suitably large value of θ as shown in Fig. 1, the resonances are isolated from the 2θ-rotated lines of continuum states and can be identified clearly. These eigenstates also satisfy the extended completeness relation (ECR) [20,21], consisting of bound states, resonances, and rotated continua for the state index n as

$$1 = \sum_n |\chi_n^\theta\rangle\langle\tilde{\chi}_n^\theta|, \tag{10}$$

where $\{\tilde{\chi}_n^\theta, \chi_n^\theta\}$ form a set of biorthogonal bases [20]. This relation is important when we describe the scattering states with the Lippmann-Schwinger equation.

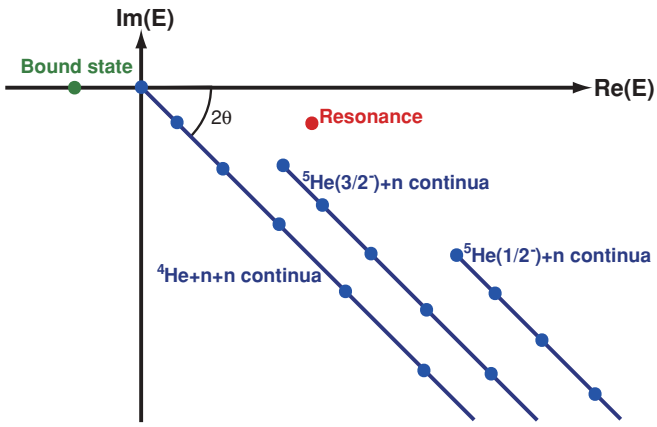

FIG. 1. (Color online) Schematic picture of energy spectra for ^{6}He in CSM, measured from the ^{4}He $+ n + n$ threshold.

In the many-body case of CSM, energy eigenvalues of rotated continuum states are classified into several groups of the different decay modes. For ^{6}He, energies of continuum states are located on the 2θ-rotated lines starting from different thresholds of two- and three-body decay channels, such as ^{5}He $+ n$ and ^{4}He $+ n + n$, as shown in Fig. 1. This classification implies that an outgoing boundary condition of each decay mode is automatically imposed for each wave function via their imaginary part of energy eigenvalue. Hence, CSM makes it possible to describe many-body scattering states without any explicit enforcement of boundary conditions.

C. Complex-scaled solutions of the Lippmann-Schwinger equation and $E1$ transition

We used the CSLS to obtain the three-body scattering states. A basic explanation of this method is given in Ref. [22]. In CSLS, we start with the formal solution of the Lippmann-Schwinger equation given as

$$\Psi^{(\pm)} = \Phi_0 + \lim_{\varepsilon\to 0}\frac{1}{E - \hat{H} \pm i\varepsilon}\hat{V}\Phi_0, \tag{11}$$

where Φ_0 is a solution of the asymptotic Hamiltonian $\hat{H}_0$. The total Hamiltonian $\hat{H}$ is the same as in Eq. (3). The interaction $\hat{V}$ is obtained by subtracting $\hat{H}_0$ from $\hat{H}$.

For the three-body breakup of ^{6}He into $\alpha + n + n$, the asymptotic Hamiltonian $\hat{H}_0$ is defined as the kinetic operator for the three-body system because there is no binary bound system in the $\alpha + n + n$ system. We also obtain the solution of the asymptotic Hamiltonian $\hat{H}_0$ as

$$\hat{H}_0 = \sum_{i=1}^{3} t_i - T_{\text{c.m.}}, \tag{12}$$

$$\hat{H}_0\Phi_0 = \left(\frac{\hbar^2 k^2}{2\mu} + \frac{\hbar^2 K^2}{2M}\right)\Phi_0 \tag{13}$$

$$\langle \mathbf{r}, \mathbf{R}|\Phi_0(\mathbf{k}, \mathbf{K})\rangle = \frac{1}{(2\pi)^3}e^{i\mathbf{k}\cdot\mathbf{r}+i\mathbf{K}\cdot\mathbf{R}}, \tag{14}$$

where $\mathbf{k}$ and $\mathbf{K}$ represent relative momenta of the asymptotic region for the three-body decays, and μ and M are reduced masses corresponding to $\mathbf{k}$ and $\mathbf{K}$, respectively. The Jacobi relative coordinates $\mathbf{r}$ and $\mathbf{R}$ are conjugates to the relative momenta $\mathbf{k}$ and $\mathbf{K}$, respectively. The interaction $\hat{V}$ in Eq. (11) is also given as

$$\hat{V} = \sum_{i=1}^{2} V_{\alpha n}(\mathbf{r}_i) + V_{nn} + V_{\alpha nn}. \tag{15}$$

The pseudopotential V_{PF} is considered in the calculations of all of the eigenstates in ECR of Eq. (10) including the ground state. In Eq. (11), we dropped V_{PF} from the interaction $\hat{V}$ to avoid the instability of the numerical results, which comes from the large number of $\lambda = 10^6$ MeV, in the calculation of the three-body scattering states.

Here, we consider the incoming scattering states $\Psi^{(-)}$ in the bra representation, which is used in the calculation of the

$E1$ transition. Equation (11) is rewritten as

$$\begin{aligned}&\langle\Psi^{(-)}(\mathbf{k},\mathbf{K})|\\&\quad=\langle\Phi_0(\mathbf{k},\mathbf{K})|+\langle\Phi_0(\mathbf{k},\mathbf{K})|\left(\lim_{\varepsilon\to0}\frac{1}{E-\hat{H}-i\varepsilon}\hat{V}\right)^{\dagger}\\&\quad=\langle\Phi_0(\mathbf{k},\mathbf{K})|+\langle\Phi_0(\mathbf{k},\mathbf{K})|\hat{V}\lim_{\varepsilon\to0}\frac{1}{E-\hat{H}+i\varepsilon}.\end{aligned}\tag{16}$$

In the derivation of the last line, we assume the Hermiticities of $\hat{H}$ and $\hat{V}$. To represent the state $\Psi^{(-)}$, it is required to calculate the Green's function in Eq. (16).

In CSLS, we use the complex-scaled Green's function [20,22]. The complex-scaled Green's function with outgoing boundary conditions, $\mathcal{G}^{\theta}(E)$, is related to a nonscaled Green's function $\mathcal{G}(E)$ as follows:

$$\lim_{\varepsilon\to0}\frac{1}{E-\hat{H}+i\varepsilon}=\mathcal{G}(E)=U^{-1}(\theta)\mathcal{G}^{\theta}(E)U(\theta).\tag{17}$$

The explicit form of $\mathcal{G}^{\theta}(E)$ is defined as

$$\mathcal{G}^{\theta}(E)=\frac{1}{E-\hat{H}^{\theta}}=\sum_n\frac{|\chi_n^{\theta}\rangle\langle\tilde{\chi}_n^{\theta}|}{E-E_n^{\theta}},\tag{18}$$

where the ECR defined in Eq. (10) is inserted in Eq. (18). Using the relation given in Eq. (18), we obtain the incoming scattering state $\Psi^{(-)}$ in Eq. (16) as

$$\begin{aligned}\langle\Psi^{(-)}(\mathbf{k},\mathbf{K})|=\langle\Phi_0(\mathbf{k},\mathbf{K})|+\sum_n\langle\Phi_0(\mathbf{k},\mathbf{K})|\hat{V}U^{-1}(\theta)|\chi_n^{\theta}\rangle\\\times\frac{1}{E-E_n^{\theta}}\langle\tilde{\chi}_n^{\theta}|U(\theta).\end{aligned}\tag{19}$$

We refer to this solution of Eq. (19) as the CSLS.

The scattering wave function in Eq. (19) consists of two terms. The first term describes the noninteracting continuum state and the second one contains all information of FSI. Using this scattering wave function, we can discuss how important each contribution is in the $E1$ transition. When the first term gives a dominant contribution in the transition, this is similar to the Fourier transformation of the ground-state wave function as discussed in the one-neutron halo systems, ^{11}Be [29] and ^{19}C [30], and hence, we can examine whether we can directly observe the signature of the ground-state correlation such as the dineutron in the Coulomb breakup. However, when the second term is dominant, FSI plays an important role in the Coulomb breakup.

We calculate the $E1$ transition strength distribution into the three-body scattering states $\Psi^{(-)}(\mathbf{k},\mathbf{K})$. First, a momentum distribution of the outgoing particles in the three-body breakup is given as

$$\frac{d^6B(E1)}{d\mathbf{k}d\mathbf{K}}=\frac{1}{2J_{\rm gs}+1}|\langle\Psi^{(-)}(\mathbf{k},\mathbf{K})||\hat{O}(E1)||\Phi_{\rm gs}\rangle|^2,\tag{20}$$

where $\Phi_{\rm gs}$ and $\Psi^{(-)}(\mathbf{k},\mathbf{K})$ are the wave functions for the initial ground and the final scattering states of ^{6}He, respectively. The spin of the ^{6}He ground state is $J_{\rm gs}$. In the three-body model of ^{6}He, protons are included only in the α core. Hence, the $E1$ transition operator $\hat{O}(E1)$ depends on the relative coordinate $\mathbf{R}_{c\text{-}2n}$ between the α core and the center of mass of the two neutrons. This is a recoil effect. The explicit form of $\hat{O}(E1)$ is given as

$$\hat{O}_m(E1)=\tfrac{2}{3}eR_{c\text{-}2n}\mathrm{Y}_{1m}(\hat{\mathbf{R}}_{c\text{-}2n}),\tag{21}$$

where m is the z component of the operator. The strength defined in Eq. (20) is the distribution with respect to two relative momenta $\mathbf{k}$ and $\mathbf{K}$ of the three-body breakups.

Second, we calculate the two-dimensional energy distribution defined as

$$\begin{aligned}\frac{d^2B(E1)}{d\varepsilon_1d\varepsilon_2}=\iint d\mathbf{k}d\mathbf{K}\frac{d^6B(E1)}{d\mathbf{k}d\mathbf{K}}\\\times\delta\left(\varepsilon_1-\frac{\hbar^2k^2}{2\mu}\right)\delta\left(\varepsilon_2-\frac{\hbar^2K^2}{2M}\right),\end{aligned}\tag{22}$$

where ε_1 and ε_2 are the relative energies of each subsystem, such as n-n and α-n of ^{6}He. Similarly, the total energy distribution of the $E1$ strength is given as

$$\frac{dB(E1)}{dE}=\iint d\mathbf{k}d\mathbf{K}\frac{d^6B(E1)}{d\mathbf{k}d\mathbf{K}}\delta\left(E-\frac{\hbar^2k^2}{2\mu}-\frac{\hbar^2K^2}{2M}\right).\tag{23}$$

Using Eqs. (22) and (23) and the equivalent photon method [31,32], we can obtain the Coulomb breakup cross sections. The two-dimensional energy distribution of the cross section and the differential cross section with respect to the total excitation energy are obtained as

$$\frac{d^2\sigma}{d\varepsilon_1d\varepsilon_2}=\frac{16\pi^3}{9\hbar c}N_{E1}(E_\gamma)\frac{d^2B(E1)}{d\varepsilon_1d\varepsilon_2}\tag{24}$$

and

$$\frac{d\sigma}{dE}=\frac{16\pi^3}{9\hbar c}N_{E1}(E_\gamma)\frac{dB(E1)}{dE},\tag{25}$$

respectively. Here, $N_{E1}(E_\gamma)$ is the virtual photon number with the photon energy E_γ, which is given as

$$E_\gamma=\varepsilon_1+\varepsilon_2+S_{2n}=E+S_{2n},\tag{26}$$

where S_{2n} is the two-neutron separation energy of ^{6}He. The virtual photon number depends on the minimal value of the impact parameter [31,32]. In this calculation, we take this minimal value as 9.6 fm, which is the same as used in the experiment [9].

From Eq. (24), the invariant mass spectra for binary subsystems such as of α-n and n-n is given as

$$\frac{d\sigma}{d\varepsilon_1}=\int d\varepsilon_2\frac{d^2\sigma}{d\varepsilon_1d\varepsilon_2},\tag{27}$$

where ε_1 is the relative energy of the binary subsystem.

We calculate these distributions of the $E1$ strength and the cross section and discuss the relation between their structures and the correlations of the n-n and α-n subsystems in ^{6}He.

TABLE I. Obtained ground-state properties of ^{6}He.

	Hybrid-VT	Exp.
S_{2n} (MeV)	0.975	0.975[a]
$R_{\rm m}$ (fm)	2.46	2.48 ± 0.03[b]
		2.33 ± 0.04[c]
		2.50[d]
$R_{\rm ch}$ (fm)	2.04	2.068(11)[e]
$R_{c\text{-}2n}$ (fm)	3.49	
R_{nn} (fm)	4.70	
$\langle\theta\rangle$ (deg.)	67.9	
$S(E1)$ (e^2 fm^2)	1.30	1.2 ± 0.2[f]

[a]Reference [33].
[b]Reference [34].
[c]Reference [35].
[d]Reference [36].
[e]Reference [37].
[f]Reference [9].

III. RESULTS

A. Ground-state properties of ^{6}He

Before discussing the $E1$ transition of ^{6}He, we show the ground-state properties of ^{6}He obtained in the present model. In Table I, we list the separation energy of two neutrons (S_{2n}), the matter and charge radii ($R_{\rm m}$ and $R_{\rm ch}$), core-2n and n-n distances ($R_{c\text{-}2n}$ and R_{nn}), the mean opening angle $\langle\theta\rangle$ between two neutrons with respect to the core, and the nonenergy weighted sum rule value of the $E1$ transition [$S(E1)$]. The obtained results of the ground state are in a good agreement with the experiment. This fact indicates the reliability of the present model of ^{6}He.

We also calculate the density distribution of the two halo neutrons, which is useful for recognizing the dineutron correlation in ^{6}He. The two-neutron density distribution is defined as

$$\rho(r_{\alpha\text{-}n},\theta) = \langle\Phi_{\rm gs}|\delta(r_1 - r_{\alpha\text{-}n})\delta(r_2 - r_{\alpha\text{-}n})\delta(\theta_{12} - \theta)|\Phi_{\rm gs}\rangle, \tag{28}$$

where r_1 (r_2) represents a distance between the α core and the first (second) neutron and θ_{12} the opening angle between the two neutrons. The calculated two-neutron density distribution is shown in Fig. 2. One of the enhancements of the density found in the region of $\theta < 90^\circ$ represents the dineutron correlation. Another enhancement found in the region of $\theta > 90^\circ$ represents the cigar-type correlation for the position of two neutrons [1,4].

B. $E1$ excitations of ^{6}He

We first show the Coulomb breakup cross section with respect to the excitation energy of ^{6}He. This cross section is calculated using Eq. (25) and considers the experimental resolution [9]. The target is Pb and the incident energy of the ^{6}He projectile is 240 MeV/nucleon. In Fig. 3, we show the obtained cross section. It is found that there exists a low-energy enhancement in the distribution at around 1 MeV measured from the three-body threshold. This energy is just above

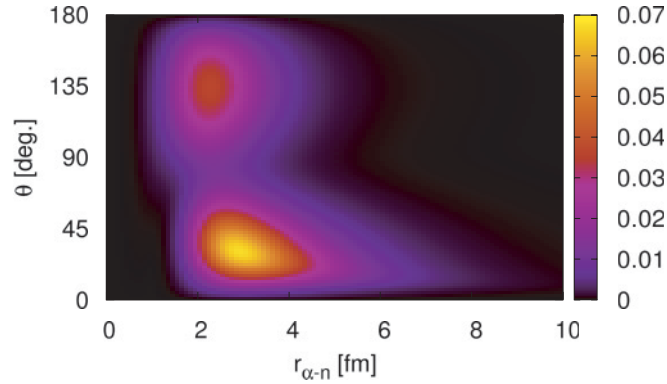

FIG. 2. (Color online) Obtained two-neutron density distribution of ^{6}He.

the two-body threshold (0.74 MeV) of the ^{5}He$(3/2^-) + n$ system [5], and the cross section gradually decreases with the excitation energy. We also compare the cross section with experiments [9] and the obtained result fairly reproduces the observed cross section, especially in the low-excitation-energy region below $E \sim 2$ MeV. The height and position of the low-energy enhancement in the strength agree well with the experiment. This means that the low-energy strength comes dominantly from the $E1$ transition. This result is also consistent with our previous analysis [20]. In Ref. [20], the factor of $1/2$ is missed in the calculation of the $E1$ transition and the minimal value of the impact parameter is different from that used in the present analysis. Using the same condition, the obtained cross sections in Ref. [20] and the present analysis are consistent with each other.

Next, we calculate the two-dimensional energy distributions using Eq. (22). These distributions are useful for seeing the correlations of the subsystem more directly than the total energy distribution, because the distributions are represented as functions of the eigenenergies of the subsystems. In Fig. 4, we show two types of the two-dimensional energy distributions with different sets of Jacobi coordinates of the three-body decay. In Fig. 4(a), we show the two-dimensional energy distribution as function of the relative energies in the α-n subsystem and between the other neutron and the center of mass of the α-n subsystem. From Fig. 4(a), it is confirmed that the strength shows an enhancement at $E_{\alpha\text{-}n} \sim 0.7$ MeV,

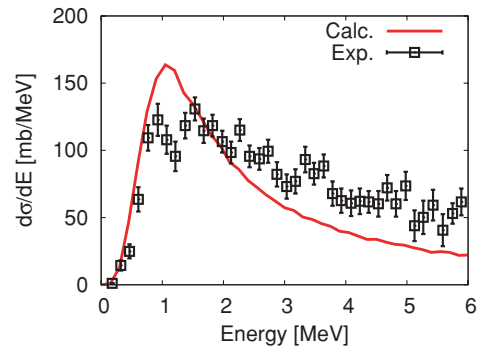

FIG. 3. (Color online) Coulomb breakup cross section measured from the $\alpha + n + n$ threshold energy, convoluted by the experimental resolution [9]. The experimental data [9] are shown as open squares.

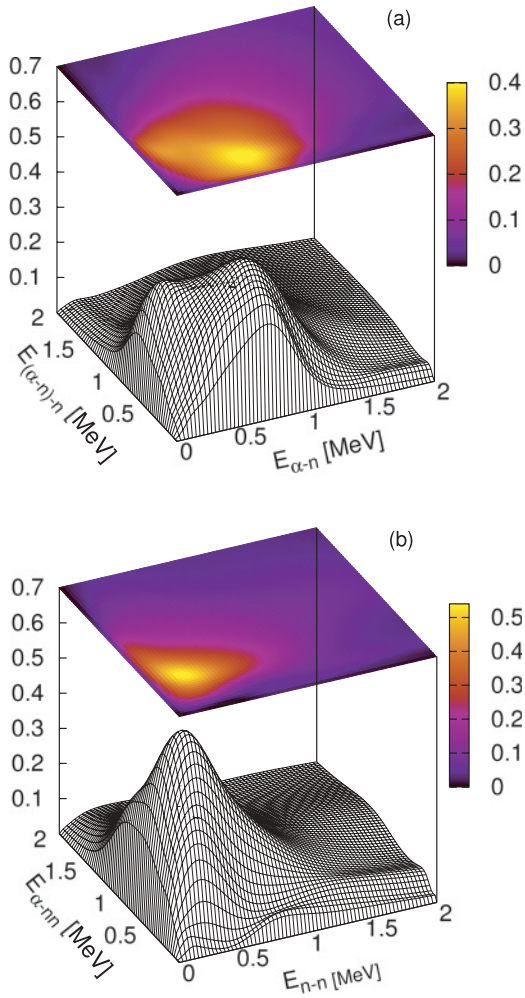

FIG. 4. (Color online) Two-dimensional energy distributions of the $E1$ strength for ^{6}He. Panel (a) shows the distribution as a function of the relative energies in the α-n subsystem and between the other neutron and the center of mass of the α-n subsystem. Panel (b) shows that as function of the relative energies in the n-n subsystem and between the α core and the center of mass of the n-n subsystem.

which corresponds to the ^{5}He$(3/2^-)$ resonance with a $p_{3/2}$ neutron. This fact leads to the signature of the sequential breakup process of ^{6}He via the $^5\mathrm{He}+n$ channel around this energy region. In our previous work [20], we also discussed the importance of the ^{5}He resonance. In Ref. [20], we decomposed the $E1$ strength distribution for the total excitation energy into the $^5\mathrm{He}+n$ and the $^4\mathrm{He}+n+n$ components using CSM and showed the dominant transition to the $^5\mathrm{He}+n$ component, which is consistent to the present results shown in Fig. 4.

In Fig. 4(b), the distribution is shown as a function of the relative energies in the n-n subsystem and between the α core and the center of mass of the n-n subsystem. In this distribution, the strength is concentrated around $E_{n\text{-}n} = 0.2$ MeV. This indicates theexistence of the n-n virtual state of the relative s-wave component. In the next section, we discuss in detail how important this n-n correlation is in the strength. From the obtained results of the two-dimensional energy distributions, the two kinds of the different correlations of α-n and n-n are clearly recognized.

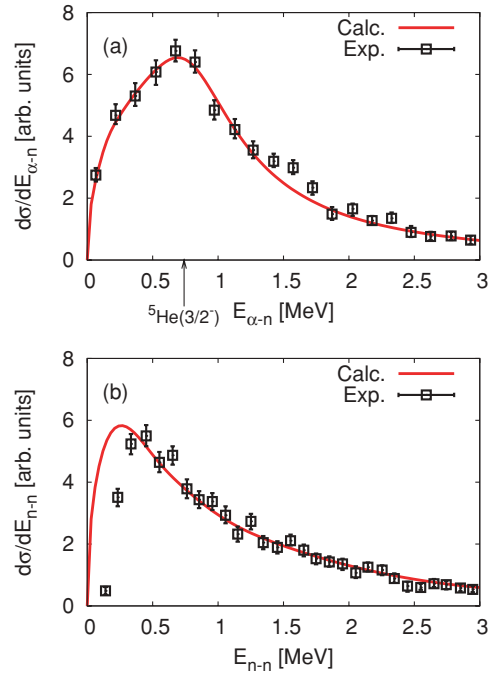

FIG. 5. (Color online) Invariant mass spectra of the Coulomb breakup cross section of ^{6}He with arbitrary units. Panels (a) and (b) represent the results with respectto the α-n and n-n binary subsystems, respectively. The open squares represent the experimental data [9]. The arrow in panel (a) indicates the ^{5}He$(3/2^-)$ resonance energy.

We also calculate two kinds of the invariant mass spectra using Eq. (27). The experimental resolution is assumed to be similar to that for the cross section in this calculation [38]. As well as the two-dimensional energy distributions, the invariant mass spectra are also useful for seeing the correlations of the subsystems. In addition, there are experimental data for the ^{6}He case [9]. In Fig. 5, we show the calculated invariant mass spectra in arbitrary units. Figures 5(a) and 5(b) show the spectra for the α-n and n-n subsystems, respectively. The two spectra obtained show good agreement with the experimental data [9]. This agreement indicates the reliability of the present CSLS method of investigating the subsystem correlation in the three-body Coulomb breakups. For the α-n case [Fig. 5(a)], it is found that the peak position of the strength coincides with the resonance energy of ^{5}He$(3/2^-)$, shown by the arrow. The ^{5}He resonance is clearly confirmed in the invariant mass spectra of the Coulomb breakup cross section. For n-n case, the low-energy enhancement is seen near the zero-energy region. These results are fully consistent with those of the two-dimensional energy distributions shown in Fig. 4. In this analysis, the calculated spectra are compared with the experimental data in arbitrary units. To investigate the subsystem correlations quantitatively, further study with the absolute value is expected for the invariant mass spectra [38].

C. Ground-state n-n correlation and n-n final-state interaction

In this section, we investigate the characteristics of the n-n correlation of ^{6}He in the Coulomb breakup strength. There are two kinds of the n-n correlations; the correlation in the ground

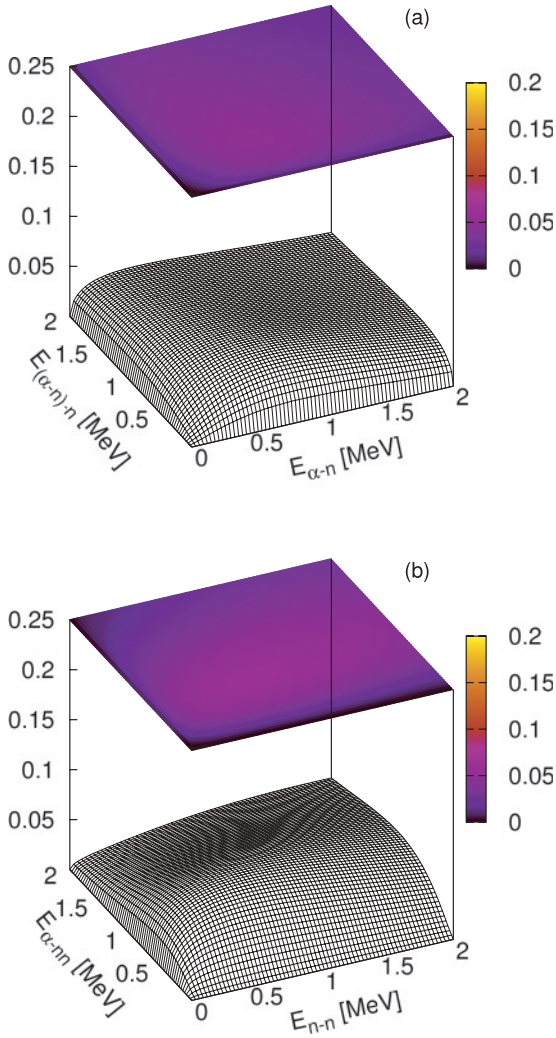

FIG. 6. (Color online) The same as Fig. 4, where only the direct breakup component is considered in the final states.

state, and that in the final scattering state. The n-n correlation in the ground state is related to the dineutron correlation as shown in Fig. 2. We discuss next whether this dineutron correlation can be observed in the breakup strength of ^{6}He.

First, to identify the ground state n-n correlation in the strength, we calculate the $E1$ strength distributions of the direct breakup component. This is the transition where there is no correlation between the constituent particles in the final state. This corresponds to the Fourier transformation of the ground state. Hence, in this case, we can look to observe a kind of signature of the ground-state correlation, such as a dineutron, in the strength. The direct breakup components are calculated by taking only the first term Φ_0 of Eq. (19) for the final-state wave function. The results of the two-dimensional energy distributions are shown in Fig. 6. It is found that the direct breakup components show the structureless distributions and give much smaller magnitudes than the results of the full calculation shown in Fig. 4. From the results obtained, we conclude that it is difficult to obtain physical information with regard to the ground-state n-n correlation from the strength of the Coulomb breakup. One cannot see a distinct signature of

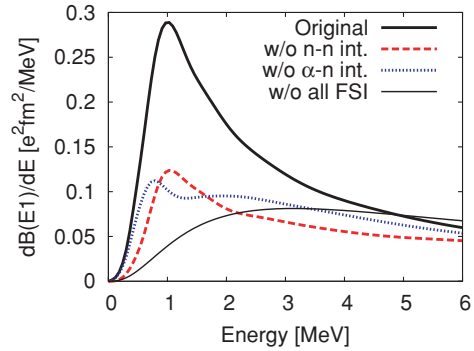

FIG. 7. (Color online) Total excitation energy distributions of the $E1$ strength of ^{6}He with and without FSIs. The black thick and thin lines show the results with and without all FSIs, respectively. The red (dashed) and blue (dotted) lines shows those without the n-n and α-n FSIs, respectively.

the dineutron correlation from the $E1$ strength of ^{6}He. This fact indicates the the strong influence of FSI in the Coulomb breakup strength, which will be discussed later in this article.

Next, we investigate the n-n FSI in the Coulomb breakup strength. Here, FSI means the operator $\hat{V}$ in the second term of Eq. (19) and is given by Eq. (15). We calculate the strength by dropping $V_{\alpha n}$ and V_{nn} to examine each contribution of the α-n and n-n FSIs, respectively. We do not consider the contribution of $V^3_{\alpha nn}$ because the effect of $V^3_{\alpha nn}$ is almost negligible in the calculation of the strength. In Fig. 7, we show the four types of the $E1$ strength distributions by changing FSI with respect to the total excitation energy of ^{6}He. The distributions with all FSIs (original), with $V_{\alpha\text{-}n}$ and without the $V_{n\text{-}n}$, without $V_{\alpha\text{-}n}$ and with $V_{n\text{-}n}$, and without all FSIs, namely, plane wave treatment of the final states.

From this comparison, none of the distributions without any FSI reproduce the original one. This means that both of the α-n and n-n FSIs contribute to construct the original strength. It is also found that the contributions of two FSIs of α-n and n-n are comparable to each other. Including the only α-n FSI (dashed), the whole shape of the $E1$ strength distribution is reproduced, while its magnitude is smaller than the original one. This indicates that the peak position of the distribution comes mainly from the sequential decay process via the $^5\mathrm{He}(3/2^-) + n$ channel, as was discussed previously. The role of the n-n FSI enhances the strength globally, without changing the shape of the distribution. In the case where we include the only n-n FSI (dotted), the strength changes its shape slightly from the original one. This is attributable to the absence of the ^{5}He resonance. From the results, the importance of the ^{5}He resonance in the final state is shown to determine the shape of the strength.

Finally, to discuss the role of the n-n FSI, we calculate the invariant mass spectrum of the $E1$ strength for the n-n subsystem by switching off the n-n FSI. In Fig. 8, the invariant mass spectrum without the n-n FSI is shown in comparison with the original one. From this comparison, it is confirmed that the peak of the spectrum is broadened because of the absence of the n-n FSI. Hence, we can understand that the low-energy enhancement observed in the original spectrum comes from the n-n FSI, not from the ground-state n-n correlation.

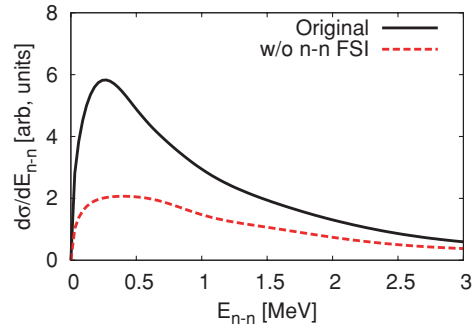

FIG. 8. (Color online) Invariant mass spectra of the $E1$ strength of ^{6}He for the n-n subsystems, respectively. The black (solid) and red (dashed) lines show the results including all FSI and without the n-n FSI, respectively.

From the results obtained, it is found that the correlations of α-n as ^{5}He and n-n systems observed in the Coulomb breakup of ^{6}He are governed by FSIs, not by the ground-state correlation. As a result, it is difficult to observe the ground-state correlation of ^{6}He using the Coulomb breakup reaction.

IV. SUMMARY

In this article, we have developed a method of investigating the three-body breakup of nuclei based on the CSM and the Lippmann-Schwinger equation. We refer to this new theoretical scheme as the CSLS. In CSLS, the boundary conditions of three-body decaying states are correctly taken intro account. We apply this method to the analysis of the three-body Coulomb breakup of the halo nucleus ^{6}He. We successfully describe the strength distributions for the total excitation energy of ^{6}He and further for the subsystem energies of α-n and n-n. We have shown that two-dimensional energy distributions and invariant mass spectra give useful information for understanding the subsystem correlations in the strength. The obtained breakup cross section also reproduces the experiment, which indicates the reliability of the CSLS approach.

From the analysis of the strength of ^{6}He, it is found that the signature of the ground-state correlation, such as a dineutron, is difficult to observe via the breakup strength. The reason is that the structure observed in the strength distributions is governed by the FSIs. In particular, the enhancement of the total energy distribution of the $E1$ strength is determined mainly by the sequential decay process via $^5\mathrm{He}(3/2^-) + n$, while the n-n FSI is also important for determining the magnitude of the whole strength. For the n-n correlation, it is shown that the distributions for the energies of the n-n subsystem are sensitive to the n-n FSI.

It would be interesting to perform a similar analysis for ^{11}Li in the next step. In ^{11}Li, the ground-state correlation is different from ^{6}He because of the large mixing of the s^2 halo component. This large s^2 mixing is expected to enhance the dineutron component in the ground state [8]. It would be interesting to investigate the dipole response of this nucleus.

ACKNOWLEDGMENTS

Y. Kikuchi thanks the members of the nuclear theory group at Hokkaido University. This work was supported by Grants-in-Aid from the Japan Society for the Promotion of Science for JSPS Fellows (No. 204495) and for Young Scientists (No. 21740194).

[1] M. V. Zhukov, B. V. Danilin, D. V. Fedorov, J. M. Bang, I. J. Thompson, and J. S. Vaagen, Phys. Rep. **231**, 151 (1993).
[2] A. Csótó, Phys. Rev. C **49**, 3035 (1994).
[3] Y. Suzuki, Nucl. Phys. A **528**, 395 (1991).
[4] S. Funada, H. Kameyama, and Y. Sakuragi, Nucl. Phys. A **575**, 93 (1994).
[5] S. Aoyama, S. Mukai, K. Katō, and K. Ikeda, Prog. Theor. Phys. **93**, 99 (1995).
[6] K. Hagino and H. Sagawa, Phys. Rev. C **72**, 044321 (2005).
[7] T. Myo, K. Katō, H. Toki, and K. Ikeda, Phys. Rev. C **76**, 024305 (2007).
[8] T. Myo, Y. Kikuchi, K. Katō, and K. Ikeda, Prog. Theor. Phys. **119**, 561 (2008).
[9] T. Aumann *et al.*, Phys. Rev. C **59**, 1252 (1999).
[10] J. Wang *et al.*, Phys. Rev. C **65**, 034306 (2002).
[11] K. Ieki *et al.*, Phys. Rev. Lett. **70**, 730 (1993).
[12] S. Shimoura, T. Nakamura, M. Ishihara, N. Inabe, T. Kobayashi, T. Kubo, R. H. Siemssen, I. Tanihata, and Y. Watanabe, Phys. Lett. B **348**, 29 (1995).
[13] M. Zinser *et al.*, Nucl. Phys. A **619**, 151 (1997).
[14] T. Nakamura, Nucl. Phys. A **788**, 243c (2007).
[15] H. Esbensen and G. F. Bertsch, Nucl. Phys. A **542**, 310 (1992).
[16] L. V. Chulkov *et al.*, Nucl. Phys. A **759**, 23 (2005).
[17] S. N. Ershov, B. V. Danilin, and J. S. Vaagen, Phys. Rev. C **74**, 014603 (2006).
[18] K. Hagino, H. Sagawa, T. Nakamura, and S. Shimoura, Phys. Rev. C **80**, 031301(R) (2009).
[19] T. Myo, K. Katō, and K. Ikeda, J. Phys. G **31**, S1681 (2005).
[20] T. Myo, K. Katō, S. Aoyama, and K. Ikeda, Phys. Rev. C **63**, 054313 (2001).
[21] T. Myo, A. Ohnishi, and K. Katō, Prog. Theor. Phys. **99**, 801 (1998).
[22] Y. Kikuchi, T. Myo, M. Takashina, K. Katō, and K. Ikeda, Prog. Theor. Phys. **122**, 499 (2009).
[23] S. Saito, Prog. Theor. Phys. **40**, 893 (1968); **41**, 705 (1969); Prog. Theor. Phys. Suppl. **62**, 11 (1977).
[24] H. Kanada, T. Kaneko, S. Nagata, and M. Nomoto, Prog. Theor. Phys. **61**, 1327 (1979).
[25] D. R. Thompson, M. LeMere, and Y. C. Tang, Nucl. Phys. A **286**, 53 (1977); Y. C. Tang, M. LeMere, and D. R. Thompson, Phys. Rep. **47**, 167 (1978).
[26] E. Hiyama, Y. Kino, and M. Kamimura, Prog. Part. Nucl. Phys. **51**, 223 (2003).
[27] S. Aoyama, T. Myo, K. Katō, and K. Ikeda, Prog. Theor. Phys. **116**, 1 (2006) , and references therein.

[28] J. Aguilar and J. M. Combes, Commun. Math. Phys. **22**, 269 (1971) ; E. Balslev and J. M. Combes, *ibid.* **22**, 280 (1971).
[29] T. Nakamura *et al.*, Phys. Lett. B **331**, 296 (1994).
[30] T. Nakamura *et al.*, Phys. Rev. Lett. **83**, 1112 (1999).
[31] B. Hoffmann and G. Baur, Phys. Rev. C **30**, 247 (1984).
[32] C. A. Bertulani and G. Baur, Phys. Rep. **163**, 299 (1988).
[33] F. Ajzenberg-selove, Nucl. Phys. A **506**, 1 (1989).
[34] I. Tanihata, T. Kobayashi, O. Yamakawa, S. Shimoura, L. Ekumi, K. Sugimoto, N. Takahashi, T. Shimoda, and H. Sato, Phys. Lett. B **206**, 592 (1988).
[35] I. Tanihata, D. Hirata, T. Kobayashi, S. Shimoura, K. Sugimoto, and H. Toki, Phys. Lett. B **289**, 261 (1992).
[36] J. S. Al-Khalili and J. A. Tostevin, Phys. Rev. C **57**, 1846 (1998).
[37] P. Mueller *et al.*, Phys. Rev. Lett. **99**, 252501 (2007).
[38] T. Aumann (private communication).